ACCURATE 3-DIMENSIONAL IMAGE RECONSTRUCTION ALGORITHM EXTENDING RPM METHOD TO ISAR MODEL

Shouhei Kidera[1], *Hiroyuki Yamada*[2] *and Tetsuo Kirimoto*[1]

[1] Graduate School of Informatics and Engineering, University of Electro-Communications, Tokyo, Japan
[2] Hitachi, Ltd. Softwave Division, Tokyo, Japan
Email: kidera@ee.uec.ac.jp

ABSTRACT

Microwave 3-dimensional reconstruction techniques exploiting multiple ISAR (Inverse Synthetic Aperture Radar) images have been well established, and are suitable for the recognition of artificial targets such as aircrafts or ships. However, the existing algorithms assume only an aggregation of multiple points, and most require the tracking of the multiple points over multiple ISAR images. In the case of a solid object with a continuous boundary, such as a wire or polyhedral structure, these algorithms severely suffer from the inaccuracy for 3-D imaging, owing to scattering centers shifting on the target surface in terms of the observation angle. To tackle the above difficulty, this paper extends RPM (Range Points Migration) method to the ISAR observation model, where a double mono-static model is introduced to suppress cross-range ambiguity. Numerical simulation demonstrates that the proposed algorithm has a distinct advantage in accurate 3-D imaging, even for not point-wise targets.

Index Terms— Accurate 3-D reconstruction, Multiple ISAR images, Solid objects with continuous boundary, RPM algorithm

1. INTRODUCTION

Microwave imaging systems are indispensable tools for geo-surface measurement or target recognition even in an optically harsh environment, such as in conditions of adverse weather or darkness. In particular, coast-guard surveillance radar strongly requires an accurate 3-D target reconstruction algorithm that can discriminate boats carrying refugees or unidentified ships. As a promising approach for objects with a discontinuous height distribution, such as buildings, aircrafts or ships, 3-D imaging algorithms based on the layover in the ISAR imagery have been developed applying high-resolution spectral estimation theory [1] or combining the interferometry basis for the 3-D inverse problems [2].

In most recent literature [3], the 3-D geometry is more accurately obtained by exploiting sequential ISAR images, so-called ISAR movies, where target points are sequentially tracked over multiple ISAR images. Although this method realizes an accurate 3-D reconstruction of an object constituted by multiple points, it is not appropriate for solid objects with continuous boundaries, such as wires or polyhedral structures. This is because (1) each scattering center on a boundary continuously shifts along the boundary in terms of rotation angle and (2) it requires a correct connection of the focused points over the multiple ISAR images.

On the contrary, several high-resolution and accurate 3-D imaging algorithms for near-field UWB (Ultra Wideband) radar have been developed [4, 5]. One of the most flexible and accurate imaging tools, the RPM algorithm, has been established [5], which is applicable to complex-shaped or multiple objects. Notably, this method directly estimates an accurate DOA (direction of arrival) employing statistical properties for the range point distribution, and does not require their connection.

With this background, the present paper newly introduces a 3-D imaging algorithm by extending the original RPM algorithm [5] to a rotating target model. In addition, this study employs a double mono-static model to suppress cross-range ambiguity in imaging. Furthermore, the extended RPM divides the range points into two types to enhance imaging accuracy in each cross-range compression. Numerical simulation with a 1/100 downscale model shows that the proposed method accomplishes accurate 3-D reconstruction of a target even for an object with a continuous boundary.

2. OBSERVATION MODEL

Figure 1 shows the system model. It assumes mono-static radar, and an omni-directional antenna is set at $(x_1, 0, z_0)$. The model also assumes that a target has arbitrary shape (e. g. multiple points or a general solid object) and is at $z \leq z_0$, for simplicity. A target rotates at a uniform angular velocity about the z axis, and its angular velocity is known. The following section deals with the equivalent observation model of an antenna scanning along a circle with radius x_1 and center $(0, 0, z_0)$ without loss of generality. The real space expressed as (x, y, z) is normalized by the central wavelength of the transmitted pulse λ.

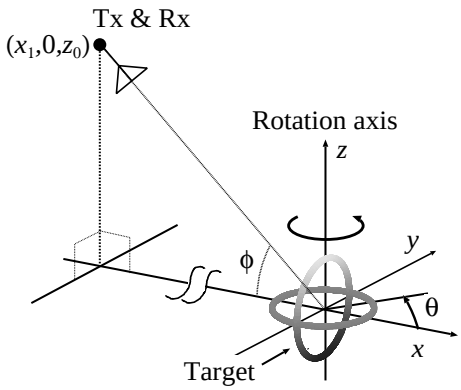

Fig. 1. System model.

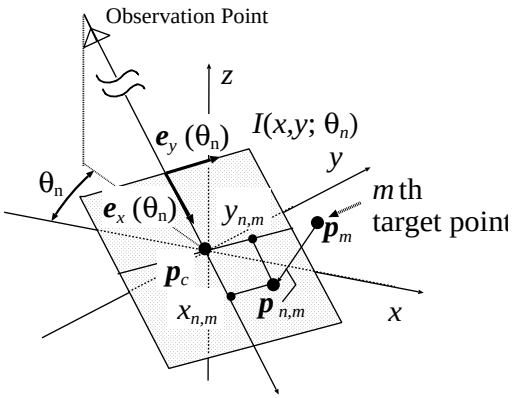

Fig. 2. Spatial relationship between the image plane and target point.

3. CONVENTIONAL METHOD

A method for high-resolution 3-D imaging based on range-Doppler azimuthal compression has been already proposed [3], which tracks the focused points over multiple ISAR images. This section briefly explains the 3-D reconstruction for this method, and states the problem exemplified by a typical example.

Here, $I(x, y; \theta_n)$ is defined as the ISAR obtained image from observation angle θ_n, $(n = 1, \cdots, N)$. The sequential images can be obtained employing PFA (Polar Format Algorithm) with low computational load [6]. The significant focused points extracted from local maxima of $I(x, y; \theta_n)$ are denoted $\boldsymbol{p}_{n,m} \equiv (x_{n,m}, y_{n,m})$. Figure 2 shows the spatial relationship between the image plane $I(x, y; \theta_n)$, and the m th target point as $\boldsymbol{p}_m$, at observation angle θ_n. This method then estimates the target point as $\hat{\boldsymbol{p}}_{n+1,m}$ in the next ISAR image on basis of the the nearest neighbor scheme;

$$\hat{\boldsymbol{p}}_{n+1,m} = \underset{\boldsymbol{p}_{n+1,m'}}{\arg\min} \|\boldsymbol{p}_{n+1,m'} - \boldsymbol{p}_c - \boldsymbol{R}(\Delta\theta)(\boldsymbol{p}_{n,m} - \boldsymbol{p}_c)\|, \tag{1}$$

where, $\boldsymbol{R}(*)$ denotes the rotation matrix for the clockwise direction, $\boldsymbol{p}_c$ is the location of the center of the assumed imaging plane $I(x, y; \theta_n)$, and $\Delta\theta$ is the interval of the rotation angles. Finally, the target's 3-D coordinates $\boldsymbol{p}_m$ are obtained by the least squared errors approach;

$$\boldsymbol{p}_m = (\boldsymbol{A}^T\boldsymbol{W}\boldsymbol{A})^{-1}\boldsymbol{A}^T\boldsymbol{W}\boldsymbol{b}_m + \boldsymbol{p}_{\mathrm{c}}, \tag{2}$$

where $\boldsymbol{W}$, $\boldsymbol{A}$ and $\boldsymbol{b}_m$ are defined as

$$\begin{aligned}\boldsymbol{W} \equiv\ & \mathrm{diag}\left[I(\boldsymbol{p}_{n,m};\theta_n), \cdots, I(\boldsymbol{p}_{n+L,m};\theta_{n+L})\right. \\ & \left. I(\boldsymbol{p}_{n,m};\theta_n), \cdots, I(\boldsymbol{p}_{n+L,m};\theta_{n+L})\right], \end{aligned} \tag{3}$$

$$\boldsymbol{A} \equiv [\boldsymbol{e}_x(\theta_n), \cdots, \boldsymbol{e}_x(\theta_{n+L}), \boldsymbol{e}_y(\theta_n), \cdots, \boldsymbol{e}_y(\theta_{n+L})]^T, \tag{4}$$

$$\boldsymbol{b}_m \equiv [x_{n,m}, \cdots, x_{n+L,m}, y_{n,m}, \cdots, y_{n+L,m}]^T. \tag{5}$$

L is the number of ISAR images used for 3-D reconstruction, $\boldsymbol{e}_x(\theta_n)$ denotes a 3-D unit vector directed from the observation point to $\boldsymbol{p}_c$, and $\boldsymbol{e}_y(\theta_n)$ is a unit vector orthogonal to $\boldsymbol{e}_x(\theta_n)$ on the imaging plane $I(x, y; \theta_n)$ as shown in Fig. 2.

Here, an example of reconstruction employing the proposed method is numerically investigated to discuss its imaging property. For simplicity, a scattered electric field for each rotation angle θ is calculated following the Born approximation as,

$$s(\theta_n, f) = \begin{cases} \displaystyle\sum_{m=1}^{M} A_m \mathrm{e}^{-\mathrm{j}\frac{4\pi f R_m(\theta_n)}{c}}, & (f_{\min} \le f \le f_{\max}), \\ 0, & (\mathrm{Otherwise}), \end{cases} \tag{6}$$

where M is the total number of point scatterers and $R_m(\theta_n)$ denotes the distance between the antenna location and the m th point scatterer. A_m is the reflection amplitude for each scatterer and is constant in this case. The total number of observation samples is 361 points for $0 \le \theta_n \le 2\pi$. $(x_1, 0, z_0) = (-150\cos\phi, 0, 150\sin\phi)$, where $\phi = \pi/6$ holds. The minimum and maximum frequencies $f_{\min}$ and $f_{\max}$ in creating the received signal, are 24 and 40 GHz, respectively. Figures. 3 and 4 illustrate the ISAR images with $\theta_n = 0$ and $\theta_n = \pi/9$, and the corresponding 3-D image obtained employing the conventional method, respectively, where the two circular objects are crisscrossed as in Fig. 1. This example clarifies a nontrivial problem that the 3-D image obtained with the conventional method suffers severely from inaccuracy, and offers only part of the target boundary. This problem mainly arises because, in the case of a target with a continuous boundary, the scattering center continuously moves along the target boundary as the target rotates. The approach for the tracking points in ISAR images is then invalid, and the imaging accuracy essentially deteriorates.

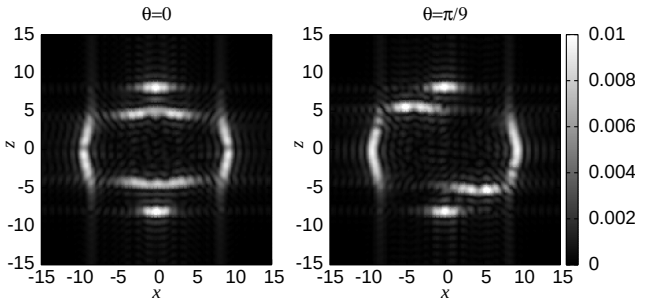

Fig. 3. ISAR images for two circular targets for $\theta = 0$ (left) and $\theta = \pi/9$.

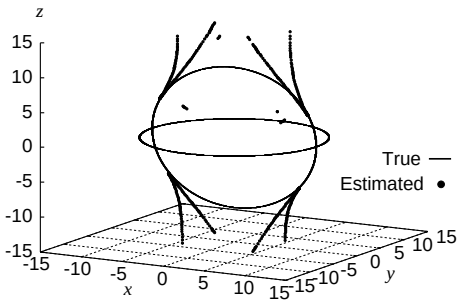

Fig. 4. 3-D reconstruction image obtained by the conventional ISAR based method.

4. RPM EXTENDED TO ISAR MODEL

As a solution to the previous problem, this paper extends the original RPM method [5] to the ISAR model. First, this extension employs two mono-static observation models as shown in Fig. 5 to avoid reconstruction ambiguity along the cross range direction. That is, the spatial interferometry between the two antennas along the x axis (antennas $\#1$ and $\#2$) is effectively used to obtain sufficient resolution in the cross-range direction. In this model, we assume that the antennas scan along two circles whose centers are $(0, 0, z_0)$ and radii are x_1 and x_2. Each antenna location is redefined as $(X, Y, z_0) \equiv (x_k \cos\theta, x_k \sin\theta, z_0), (k = 1, 2)$, and the significant range R is extracted from the local maximum of the received signal after applying the Capon method to the observation data in the frequency domain [7], and a group of "range points" $\boldsymbol{q}_i = (X_i, Y_i, R_i),\ (i = 1, \cdots, N_{\mathrm{R}})$ is obtained, where N_{R} denotes the total number of range points.

This method basically assumes that the target boundary point corresponding to $\boldsymbol{q}_i$ exists on the sphere with center (X_i, Y_i, z_0) and radius R_i. The location of the scattering point on the target for each $\boldsymbol{q}_i$ is then determined from the spatial distribution of the intersection points among the spheres

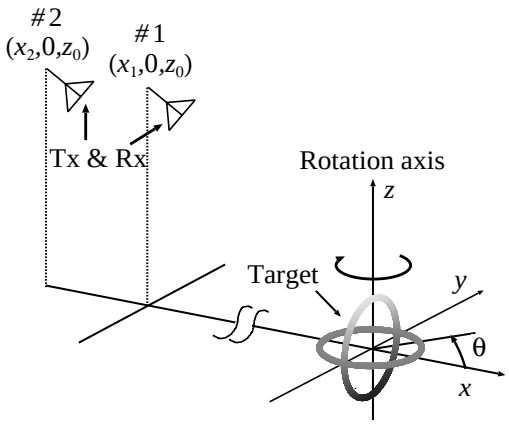

Fig. 5. System model in the proposed method.

determined for neighboring range points;

$$\hat{\boldsymbol{p}}(\boldsymbol{q}_i) = \underset{\boldsymbol{p}^{\mathrm{int}}(\boldsymbol{q}_i,\boldsymbol{q}_j,\boldsymbol{q}_k)\in\mathcal{P}_i}{\arg\max} \sum_{l=1}^{N_{\mathrm{M}}} \sum_{m=1}^{N_{\mathrm{S}}} f(\boldsymbol{p}^{\mathrm{int}}(\boldsymbol{q}_i, \boldsymbol{q}_j, \boldsymbol{q}_k)) \times \exp\left\{ -\frac{\|\boldsymbol{p}^{\mathrm{int}}(\boldsymbol{q}_i, \boldsymbol{q}_j, \boldsymbol{q}_k) - \boldsymbol{p}^{\mathrm{int}}(\boldsymbol{q}_i, \boldsymbol{q}_l, \boldsymbol{q}_m)\|^2}{2\sigma_r^2} \right\}, \quad (7)$$

where $\boldsymbol{p}^{\mathrm{int}}(\boldsymbol{q}_i, \boldsymbol{q}_j, \boldsymbol{q}_k)$ denotes the intersection point among the three circles, determined by the range points $\boldsymbol{q}_i$, $\boldsymbol{q}_j$ and $\boldsymbol{q}_k$, and $\mathcal{P}_i \equiv \left\{\boldsymbol{p}^{\mathrm{int}}(\boldsymbol{q}_i, \boldsymbol{q}_j, \boldsymbol{q}_k) | \boldsymbol{q}_j \in \mathcal{Q}_i^{\mathrm{M}}, \boldsymbol{q}_k \in \mathcal{Q}_i^{\mathrm{S}}\right\}$ holds. $\mathcal{Q}_i^{\mathrm{M}}$ expresses a set of range points, where $\sqrt{X_i^2 + Y_i^2} = \sqrt{X_j^2 + Y_j^2}$ is satisfied. σ_r is a constant empirically determined. On the other hand, $\mathcal{Q}_i^{\mathrm{S}}$ expresses a set of range points, where $\sqrt{X_i^2 + Y_i^2} \neq \sqrt{X_k^2 + Y_k^2}$ is satisfied. Fig. 6 illustrates an example of $\mathcal{Q}_i^M$, $\mathcal{Q}_i^S$ and the intersection point. The evaluation function is also defined as $f(\boldsymbol{p}^{\mathrm{int}}(\boldsymbol{q}_i, \boldsymbol{q}_j, \boldsymbol{q}_k)) \equiv s(\boldsymbol{q}_j) \exp\left\{-\frac{D(\boldsymbol{q}_i,\boldsymbol{q}_j)^2}{2\sigma_X^2}\right\} + s(\boldsymbol{q}_k) \exp\left\{-\frac{D(\boldsymbol{q}_i,\boldsymbol{q}_k)^2}{2\sigma_X^2}\right\}$, where $s(\boldsymbol{q}_j)$ is the output of the Capon, σ_X is also an empirically determined constant, and $D(\boldsymbol{q}_i, \boldsymbol{q}_j) = \sqrt{(X_i - X_j)^2 + (Y_i - Y_j)^2}$. This method has the distinct advantage that it does not require the linking of range points, and realizes accurate 3-D imaging even for targets of complex-shape.

5. PERFORMANCE EVALUATION

A numerical example of applying the proposed 3-D reconstruction method is presented. The same signal model as in Eq. (6) is used in this case. Figures. 7 and 8 are respectively 3-D images obtained employing the proposed method in the noiseless case and in the case of S/N=20dB. Here, S/N is defined as the ratio of the average signal power to that of noise in the frequency domain. $\sigma_X = 20\lambda$ and $\sigma_r = 0.5\lambda$ are set. The figures prove that the proposed method obtains an accurate image around the whole region of the target, by exploiting a

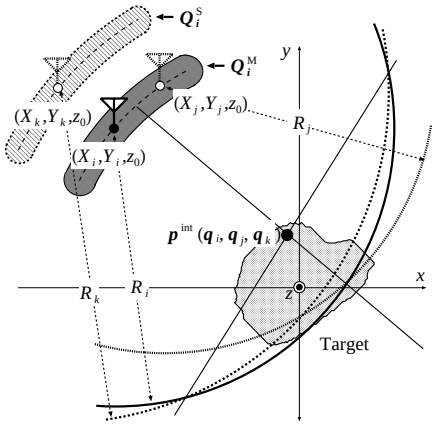

Fig. 6. Spatial relationship among antennas and intersection point.

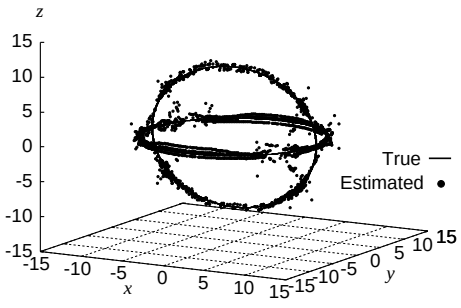

Fig. 7. 3-D reconstruction image obtained by the proposed method in noiseless situation.

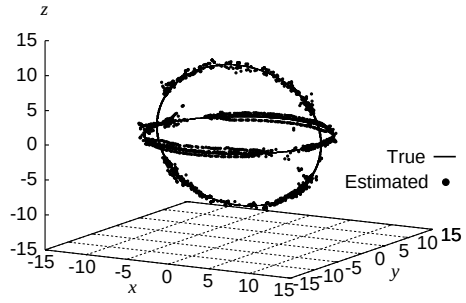

Fig. 8. 3-D reconstruction image obtained by the proposed method at S/N=20dB.

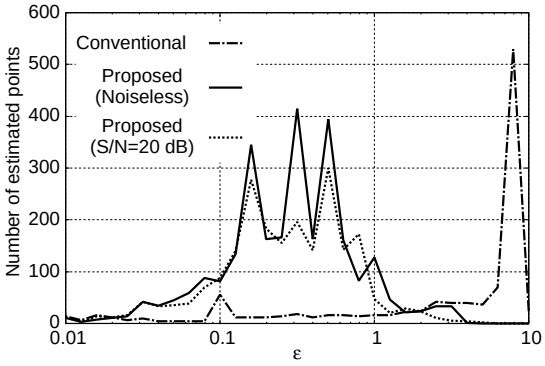

Fig. 9. Histogram of target points for each error ϵ_i.

global characteristic of the range points instead of connecting them. Here, quantitative analysis employs ϵ_i, which is defined as

$$\epsilon_i = \min_{\boldsymbol{p}_{\mathrm{true}}} \|\boldsymbol{p}_{\mathrm{true}} - \boldsymbol{p}_{\mathrm{e}}^i\|, \quad (i = 1, 2, ..., N_{\mathrm{T}}), \tag{8}$$

where $\boldsymbol{p}_{\mathrm{true}}$ and $\boldsymbol{p}_{\mathrm{e}}^i$ are the locations of the true and estimated target points, respectively. N_{T} is the total number of $\boldsymbol{p}_{\mathrm{e}}^i$. Figures 9 plots the number of estimated points for each value of ϵ in the cases of Figs. 4, 7 and 8. The mean value of ϵ_i as $\bar{\epsilon}$ is 4.61λ for the conventional method, 0.39λ and 0.35λ for the proposed method in noiseless and S/N=20dB cases, respectively. Note that, the reconstruction range in noisy situation is smaller than that in noisy situations, which causes slight accuracy improvement from the noiseless situation. This result quantitatively demonstrates the effectiveness of the proposed method for accurate 3-D imaging, even for an object with a continuous boundary.

6. CONCLUSION

This paper proposed a novel 3-D reconstruction algorithm by extending the original RPM algorithm to the ISAR model. In this extension, a double mono-static model is introduced to suppress cross-range ambiguity. The notable advantage of this method is that it is applicable to an object with a continuous boundary, for which a scattering center shifts along the target boundary. A numerical result confirmed that our method remarkably enhances accuracy in 3-D target reconstruction, even at lower S/N.

7. REFERENCES

[1] J. Mayhan, M. Burrows, K. Cuomo and J. Piou, *IEEE Trans. Aerosp. Electron. Syst.*, vol. 37, no. 2, pp. 630–642, Apr. 2001.

[2] X. Xu and R. M. Narayanan, *IEEE Trans. Image Processing*, vol. 10, no. 7, pp. 1094–1102, Jul. 2001.

[3] M. Iwamoto and T. Kirimoto, *in Proc. IEEE IGARSS*, Jul. 2001, vol. 4, pp. 1607–1609.

[4] T. Sakamoto, *IEICE Trans. Commun.*, vol.E90-B, no.3, pp. 636–644, 2007.

[5] S. Kidera, T. Sakamoto and T. Sato, *IEEE Trans. Geosci. Remote Sens.*, vol. 48, no. 4, pp. 1993-2004, Apr., 2010.

[6] W. G. Carrara, R. S. Goodman and R. M. Majewski, *Artech House*, 1995.

[7] S. Kidera, T. Sakamoto and T. Sato, *IEEE Trans. Antenna Propagat.*, vol. 59, no. 5, pp. 1606–1615, May, 2011.